PARTICLE SEPARATION IN MICROFLUIDIC DEVICES

— SPLITT Fractionation and Microfluidics

Yonghao Zhang*, Robert W. Barber, David R. Emerson

Centre for Microfluidics and Microsystems Modelling, CCLRC Daresbury Laboratory, Daresbury, Warrington, Cheshire, WA4 4AD, UK

* Corresponding author: Tel: +44-1925-603149; Fax: +44-1925-603634; E-Mail: Y.Zhang@dl.ac.uk

Abstract

In recent years, microfluidic devices have been increasingly used to separate particles such as colloids, macromolecules, cells, beads and droplets. Miniaturized devices can introduce new functionalities and experimental paradigms that are not possible at conventional macroscopic scales. In this paper, split-flow-thin (SPLITT) fractionation techniques, which may help to develop integrated microfluidic devices for particle separation, are briefly reviewed. The underlying physics of particle migration will be discussed and the advantages of numerical simulation for rational microfluidic device design and operation are highlighted.

Key words: SPLITT fractionation, microfluidics, particle separation.

1. INTRODUCTION

Microfluidic devices have been developing rapidly since the concept of fluid-integrated-circuit, lab-on-a-chip or micro-total-analysis systems (μTAS) was introduced [1, 2]. Among the great benefits of miniaturised devices are that they require less fabrication material and can also be manufactured as cheap disposable test kits. They consume smaller amounts of expensive reagents in comparison to conventional macro-scale devices and can control temperature and other system properties precisely. Miniaturised systems can increase yields significantly in chemical, biological and clinical applications and can also reduce process time. More importantly, micro-devices can have additional functionalities beyond those of conventional devices, with the potential to revolutionise many scientific areas and associated industries [3]. The design, fabrication and application of μTAS has attracted researchers from various disciplines including chemistry, biology, physics, engineering and applied mathematics. Recent general developments in this area have been discussed in a number of review articles [4-9].

Miniaturisation has produced new experimental paradigms for particle separation due to the enhanced functionalities these devices offer. One such example is the H-filter, shown in Fig. (**1**), which was developed by Yager and his colleagues [10]. The H-filter was originally designed to allow a continuous extraction of molecular analytes from fluids containing larger particles. The filter output was preferentially enriched with smaller (faster diffusing) molecules. The applications include blood plasma separations, PCR product clean-up, artificial kidneys and drug discovery. This diffusion-based particle separation device will only work at the micro-scale. For example, small particles like haemoglobin in water normally take about 300 hours to diffuse 1 cm, but only around 1 second to diffuse 10 μm. However, larger particles, such as red blood cells, need about 10 minutes to diffuse 10 μm. The smaller haemoglobin particles will readily move across the stream to the filter output and be separated from the larger red blood cells.

Yager [11] pointed out that Giddings and his colleagues had already invented a diffusion-based split-flow-thin (SPLITT) fractionation device, shown in Fig. (**2**), which employed the same methodology as the H-filter. SPLITT fractionation techniques have been well developed and various particle driving

mechanisms including electrical, gravitational, magnetic and ultrasonic fields have been explored. In section 2, SPLITT fractionation techniques are briefly reviewed which may guide researchers in the development of integrated particle separation components in μTAS. The emphasis of section 2 is on the use of magnetic fields for particle separation which are becoming increasingly popular in biological and clinical analyses.

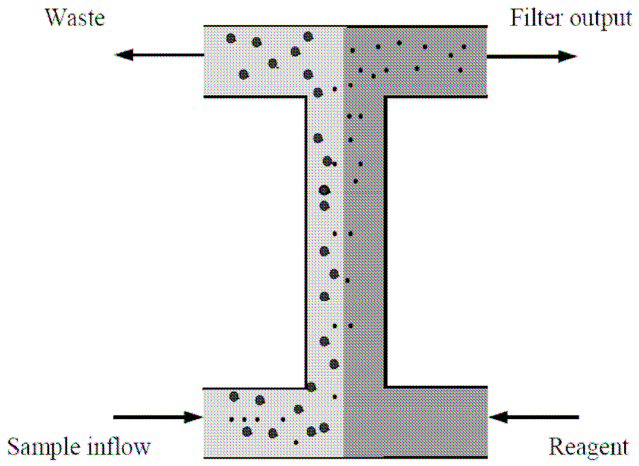

Fig. (**1**). Schematic representation of an H-filter.

Particle-laden flows in micro-devices differ in many respects from conventional flows. For example, microflows are usually laminar and the Stokes number is often small. These unique features can be exploited to build novel microfluidic devices. The fundamentals of the underlying physics of particle separation will therefore be discussed in section 3. Finally, section 4 illustrates how numerical simulations based on the physical models of particle separation can be used to improve "trial and error" methodologies for device design and operation. Two recent examples are given that demonstrate the potential of numerical simulations.

One aim of the present review paper is to make researchers in the field of μTAS more aware of SPLITT fractionation techniques for particle separation which may be beneficial in the further development of μTAS. The other aim is to help researchers who are unfamiliar with numerical simulation to better

understand the physics of particle motion in microfluidic devices and to take full advantage of the many sophisticated software packages that can improve microfluidic device design and operation.

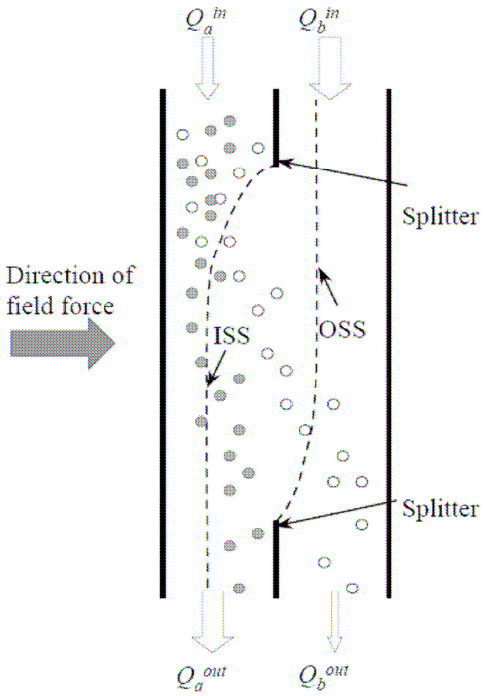

Fig. (**2**). Schematic of a SPLITT fractionation device where Q_a^{in}, Q_b^{in}, Q_a^{out} and Q_b^{out} are the flow rates at inlets *a*, *b* and outlets *a*, *b* respectively. *ISS* and *OSS* refer to two imaginary inlet and outlet splitting streamlines.

2. SPLITT FRACTIONATION

Before the introduction of μTAS, a family of SPLITT fractionation techniques had already been developed employing separation methods that are now being used in current integrated microsystems. SPLITT fractionation is an extension of field-flow fractionation (FFF). The FFF approach was one of the earliest microfluidic techniques to be used for particle separation [12]. FFF methods were first introduced by Giddings in the 1970s and a range of FFF devices have subsequently been demonstrated [13]. In the 1980s, Giddings [14] proposed the concept of SPLITT fractionation for the continuous separation of particles and a diagram of a typical SPLITT device is shown in Fig. (**2**). A field perpendicular to the flow direction is applied to force the particles to migrate. Generally, a device will have two inlets and two outlets with controlled, but different, flow rates. The two inflows merge at the inlet splitter and the flow is

separated again at the outlet splitter. Under the influence of an externally applied field, particles with higher mobility in a sample solution entering inlet *a* will be collected from outlet *b*. SPLITT fractionation techniques have been used widely in biological, medical, environmental and industrial applications [15-19]. A major advantage of SPLITT fractionation is that its continuous operation can be exploited for integrated μTAS.

SPLITT fractionation devices have different operating modes according to the driving force used for particle separation. Gravitational sedimentation has been used most frequently [15, 20-22] but many other operating modes have also been developed e.g. concentration gradient [23], centrifugal force [24], lift force [25], and electric field [26]. Interested readers are referred to the review article on SPLITT fractionation techniques by Myers [27].

Magnetic separation methods are increasingly being incorporated in μTAS. Magnetic separation usually involves magnetic carrier particles that will respond to magnetic fields and field gradients. When magnetic particles are subjected to a magnetic field, they will move relative to the other species. This method has the advantage of high selectivity due to the large difference between the permeability of the magnetic and non-magnetic materials. One of the earliest successful applications was blood cell separation which exploited the high magnetic susceptibility of iron present in haemoglobin molecules [28]. Magnetic separation techniques have now emerged as one of the preferred methods for biological and clinical analyses because of the development of new magnetic beads with improved properties [29]. For example, immunomagnetic separation has become popular for the separation of specific macromolecules and cells from heterogeneous biological mixtures [30, 31]. The manipulation of magnetic beads on-chip was recently reviewed by Gijs [32]. Magnetic fields have also been exploited in SPLITT fractionation devices and similar methodologies could therefore be useful to researchers developing chip-based magnetic separation devices.

Both dipole and quadrupole magnets have been used in SPLITT fractionation devices [17, 33-39]. The main applications have been biomedical analyses based on differences in the intrinsic and extrinsic

magnetic properties of biological macromolecules. For example, Nakamura et al. [40] tested a quadrupole magnetic flow sorter (QMS) to separate immunomagnetically-labelled breast carcinoma cells from unlabelled peripheral blood leukocytes. Recently, Wingo et al. [41] have demonstrated the separation of sub-micron paramagnetic particles using a high-gradient magnetic field. In addition to separating magnetic particles, SPLITT fractionation devices have been applied to determine the magnetic susceptibility of various ion-labelled red blood cells [42, 43]. Apart from various applications, significant effort has been made to improve the device design and operating conditions. For example, Zborowski et al. [44] have discussed the fundamentals of magnetic cell separation while Hoyos et al. [45] carried out a validation study on QMS using monodisperse magnetic beads to verify the operational theory developed by Williams et al. [46].

Not only can magnetic beads be manipulated by a magnetic field but non-magnetic particles can also be separated under a magnetic field if they are suspended in a ferrofluid. Consequently, non-magnetic particles, such as cells, do not need to be tagged by magnetic beads. A non-magnetic particle immersed in a magnetic fluid will be subjected to a magnetophoretic force under a magnetic field, which will cause the particle to migrate. Watarai et al. [47] reported the separation of polystyrene beads and blood cells from a paramagnetic salt solution. Moore et al. [48] found that the paramagnetic ion carrier can suppress the non-specific crossover in QMS for continuous separation of particles with different magnetophoretic mobility.

3. THEORETICAL CONSIDERATIONS

A theoretical understanding of particle motion in microfluidic devices not only helps to improve device design and operation but also lays down the foundation for numerical simulations. In the history of the development and application of SPLITT fractionation techniques, theory has played a very important role. For example, the flow rate optimisation theory for the QMS developed by Williams et al. [46] has greatly reduced operating costs and improved the separation efficiency. Numerical simulations can also serve as virtual experiments to diagnose factors which affect particle separation performance. “Numerical experiments” can readily investigate a wide range of design parameters including flow rates, channel dimensions, geometries and fluid properties and can identify key design and operational issues. As an

example, Williams et al. [49] numerically studied the effect of splitter imperfections on particle separation and found that small alignment errors had a significant impact, which was later confirmed experimentally [50]. Moreover, experimental costs and the development cycle can be significantly reduced. In addition, flow behaviour at the micro-scale may differ from intuitive expectation but will be captured by numerical simulation. For example, experimental measurement of particle motion at the micro-scale is difficult but numerical simulation can be used to visualise the trajectory of individual particle motions, which can be helpful in both device design and operation [51-53]. Therefore, it is important to understand the underlying physics of particle motion at the micro-scale.

3.1 CHARACTERISTICS OF FLUID-PARTICLE MOTION IN MICRO-DEVICES

Before analysing the forces acting on particles, we need to understand the basic behaviour of flow at the micro-scale. Particle-laden fluid flow can be characterised by a number of important dimensionless parameters, such as the Reynolds number and the Stokes number. The Reynolds number can be used to assess the relative importance of the inertial and viscous forces and is defined as

$$Re = \frac{\rho_f v L}{\mu} \tag{1}$$

where ρ_f is the fluid density, v is the fluid velocity, L is the characteristic length scale of the device, and μ is the fluid viscosity. The flow is generally turbulent if the Reynolds number is above 3000, while it is laminar if the Reynolds number is below 1000. For a typical micro-device with a length scale L of 100 μm transporting water with a mean velocity between 1-1000 μm/s, the Reynolds number can range between 10^{-4} and 10^{-1}. Hence, micro-flows are usually laminar with Reynolds numbers below 0.1. This indicates that scaled-down versions of conventional macroscopic devices, which generally operate at large Reynolds numbers, may not work as intended. However, the unique features of creeping laminar flow can be exploited for designing novel microfluidic devices because co-flowing fluid streams will only mix by diffusion and the flow behaviour will be highly smooth and predictable.

How quickly a particle adjusts to any change in the surrounding flow field can be related to the Stokes number, *St*, which is defined as the ratio of the particle relaxation time to the characteristic time of the flow field, i.e.

$$St = \frac{\tau_r}{\tau_f}, \tag{2}$$

where τ_r is the particle relaxation time given by

$$\tau_r = \frac{\rho_p d^2}{18\mu}, \tag{3}$$

and τ_f is the characteristic time of the flow field, which can be estimated from

$$\tau_f = \frac{L}{\langle V \rangle}. \tag{4}$$

The diameter and density of the particle are d and ρ_p, respectively, and $\langle V \rangle$ is the mean fluid velocity.

If the Stokes number is small, the particle will follow the fluid motion exactly. For example, a particle with a diameter of 10 μm and a density of 1000 kg/m^3 moving in a fluid with a viscosity of 10^{-3} Ns/m^2 has a relaxation time, τ_r, of about 10 μs. On the other hand, if the mean fluid velocity is 1 mm/s and the length scale of the device is 100 μm, the characteristic time of the flow field, τ_f, will be 0.1s. Therefore, τ_f is four orders of magnitude larger than τ_r indicating that the particle needs only a short time to adjust to changes in the surrounding flow field. The particle's acceleration, relative to the surrounding fluid, can therefore be neglected which greatly simplifies the analysis of the particle motion.

3.2 FORCES ACTING ON A PARTICLE

Small particles such as macromolecules, colloids, cells, nano-/ micro-beads, and droplets are particularly suited to manipulation in microfluidic devices. In general, a particle moving within a carrier fluid will experience a range of forces including hydrodynamic, gravity, buoyancy, as well as externally applied forces. If the forces are assumed to be linearly additive, the total force acting on the particle, Σ*F*, can be expressed by

$$\sum F = F_{drag} + F_{field} + F_{added} + F_{Basset} + F_{Saffman} + F_{Magnus} + F_g + F_b + \ldots, \tag{5}$$

where F_{drag} is the total drag force (pressure and viscous), F_{field} is the force due to an externally applied field, F_{added} is the added mass force (due to the particle entraining some of the surrounding fluid), F_{Basset} is the Basset force (a force related to the particle's history), $F_{Saffman}$ is the Saffman force (a lift force due to fluid shear), F_{Magnus} is the Magnus force (a lift force due to particle rotation), F_g is the force due to gravity, and F_b is the buoyancy force.

The size of particle is very important to the transport behaviour of micro-flows. Brownian motion may play an important role for small particles and its effect can be evaluated using the root-mean-square (RMS) displacement of an isolated spherical particle. The RMS displacement can be calculated from the Einstein-Smoluchowski equation [54]:

$$\left\langle x^2 \right\rangle^{1/2} = \sqrt{2Dt}\,, \tag{6}$$

where D is the diffusion coefficient and t is the time. In water at 25 °C, the diffusion coefficient of a spherical particle with a diameter of 0.1 μm is 4.8×10^{-12} m^2/s whereas the diffusion coefficient for a 10 μm diameter particle will be 0.048×10^{-12} m^2/s. After one second, the RMS displacement will be 3 μm for the 0.1 μm sphere but only 0.3 μm for the 10 μm sphere. Consequently, Brownian motion has a significant effect on the motion of small particles (diameter ≈ 0.1 μm or less) while it can be neglected for larger particles (diameter ≈ 10 μm or more).

The drag force acting on a rigid sphere in a steady Stokes flow, where the particle Reynolds number is small, can be determined from

$$F_{drag} = 3\pi\mu d u_r\,, \tag{7}$$

where u_r is the relative velocity between the particle and the fluid. Since most particles, including cells and macromolecules, are generally non-spherical, the drag force can be written as

$$F_{drag} = 3\pi\mu d u_r \chi\,, \tag{8}$$

where χ is known as the *dynamic shape factor*, which is the ratio of the drag force on the non-spherical particle to the drag on a sphere that occupies the same volume as the non-spherical particle.

The Saffman lift force, due to the fluid shear, can be estimated by [55]:

$$F_{Saffman} = 1.61 \mu d |u_r| \sqrt{Re_f} \,, \tag{9}$$

where Re_f is the Reynolds number based on the particle's diameter:

$$Re_f = \frac{\rho_f d^2}{\mu} |\nabla v| \,, \tag{10}$$

where ∇v is the gradient of the velocity field. The particle Reynolds number, Re_p, is defined as

$$Re_p = \frac{\rho_f d |u_r|}{\mu} \,. \tag{11}$$

If $Re_p << \sqrt{Re_f} < 1.0$, the ratio of the Saffman lift force to the drag force is given by [56]:

$$\frac{F_{Saffman}}{F_{drag}} = \frac{K}{12\pi} \sqrt{Re_f} \,, \tag{12}$$

where K is a constant with a value of 6.46. If a 10 μm diameter particle moves in an aqueous solution in a micro-device having a characteristic length scale of 100 μm and mean fluid velocity of 1 mm/s, then the Saffman lift force is typically less than 1% of the drag force. However, if the particle is subject to a flow field with a large fluid shear, such as the flow region adjacent to a wall, the lift force may be significant compared to the drag force. The Basset, Magnus, and added mass forces are generally negligible in comparison to the drag force. Moreover, if the density difference between the particle and fluid is small, gravitational and buoyancy forces usually cancel each other. Therefore, the drag and the externally applied field force are usually the most important forces controlling the motion of the particles.

The field force can be determined according to the corresponding physical mechanisms of the applied field. For example, Knoepfel [57] has shown that a particle with a magnetic permeability, μ_m, moving freely in an externally applied magnetic field, H, will experience a Kelvin force given by

$$F_m = \frac{1}{2} \nabla (B^2 / \mu_m) \delta V \,, \tag{13}$$

where B is the magnetic flux density and δV is the particle volume. The external magnetic field, H, is related to the magnetic flux density by $H=B/\mu_m$. Both B and H can be determined from Maxwell's electromagnetic field equations.

3.3 FLUID MOTION

Incompressible fluid flow can be described by the Navier-Stokes equations:

Continuity:

$$\nabla \cdot v = 0 \tag{14a}$$

Momentum:

$$\rho_f \left[\frac{\partial v}{\partial t} + (v \cdot \nabla) v \right] = -\nabla P + \mu \nabla^2 v + F_{ext}, \tag{14b}$$

where F_{ext} represents external forces, such as gravity, and P is the pressure. The momentum equation represents a force balance on an elemental volume of fluid. The left hand side contains the inertial terms while the right hand side contains terms for the pressure, viscosity and external forces. As micro-flows are usually laminar, with Reynolds numbers below 0.1, viscous forces dominate the flow and inertial forces can usually be neglected. Under these assumptions, equation (14b) reduces to Stokes' equation:

$$\nabla P = \mu \nabla^2 v + F_{ext}. \tag{15}$$

Equation (15) has the advantage of being much simpler for analytical and numerical studies in comparison with the Navier-Stokes equation.

4. NUMERICAL SIMULATIONS

Numerical models can build upon the physical understanding of fluid-particle motion discussed in section 3. If the particle concentration is small, the effect of the particle motion on the carrier fluid can be ignored [58]. Consequently, the flow field can be decoupled from the motion of the particles. The fluid flow can therefore be determined by solving the Navier-Stokes equations. Assuming the flow is also unaffected by any externally applied field, the complexity of the simulation is reduced and the applied field can be solved independently of the Navier-Stokes equations. Once all the forces acting on the particles have been determined, the motion of the particles can be solved by Newton's second law:

$$\rho_p \frac{\partial^2 x}{\partial t^2} = \frac{1}{\delta V} \sum F. \tag{16}$$

Two practical examples will be described that demonstrate how numerical simulations can be used to optimise the performance of novel field-flow fractionation devices. In this paper, the numerical

simulations have used the commercial Computational Fluid Dynamics software, CFD-ACE+ (CFD Research Corporation, Huntsville, USA) [59].

4.1 ULTRASONIC CELL WASHING SYSTEM

Ultrasonic cell washing is a continuous field-flow fractionation technique that employs an ultrasonic standing wave to migrate particles and cells. Recently, a single half-wavelength continuous flow system has been reported [60] that was used to transfer cells from one liquid medium to another (washing). A schematic view of the internal ducts is shown in Fig. (**3**) and the operating process is illustrated in Fig. (**4**). Two fluids, A and B, are injected into a rectangular cross section without mixing. Fluid A is a cell-free receiving fluid, and fluid B, is a suspension of cells. The two fluids pass through an ultrasound standing wave field that moves the cells in fluid B towards fluid A. Afterwards, the cells and their initial host fluid are removed through separate outlets.

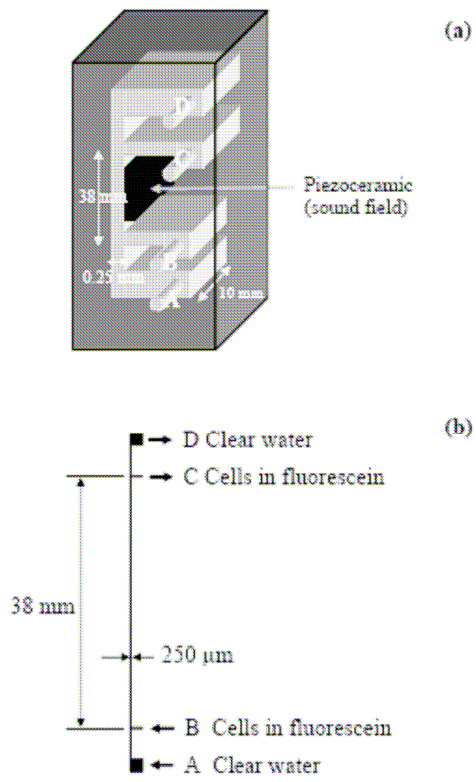

Fig. (**3**). (a) 3-D diagrammatic representation of an ultrasonic cell washing chamber (not to scale).

(b) Scale drawing of the channels in the ultrasonic chamber.

(Reproduced from Hawkes et al. [60] by permission of the Royal Society of Chemistry).

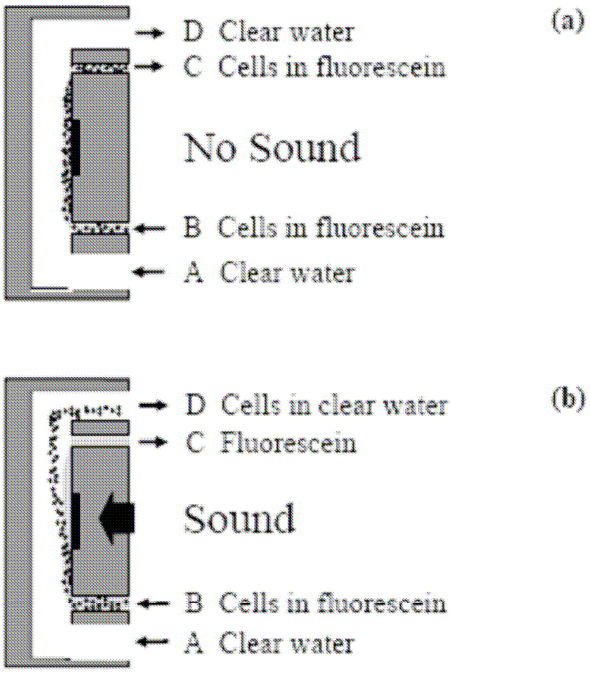

Fig. (**4**). Schematic diagram of the ultrasonic cell washing process.

(Adapted from Hawkes et al. [60] by permission of the Royal Society of Chemistry).

A high transfer of cells can be obtained when the flow rate is small. However, at low flow rates, the cell carrier fluid (fluid B) will start to mix with the receiving fluid (fluid A) due to molecular diffusion and will contaminate the sample output. The flow rate should therefore be optimised to reduce diffusive effects whilst achieving as high a cell separation as possible. Numerical simulation can be used to determine the optimum flow rate.

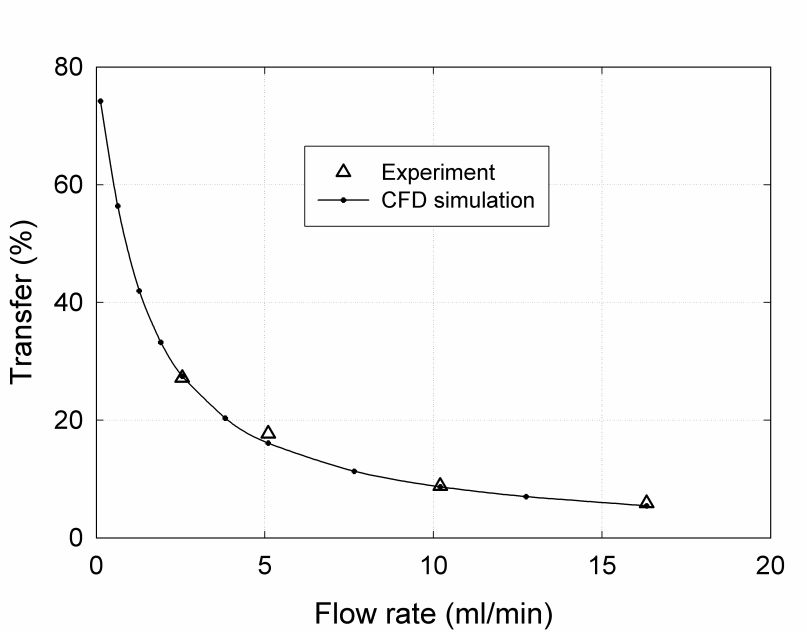

Fig. (**5**). Transfer of sodium fluorescein as a function of total flow rate. Experiments conducted using constant flow rate ratios, i.e. $Q_A/Q_B = 5$ and $Q_D/Q_C = 2.92$ where Q_A, Q_B, Q_C and Q_D are the flow rates at the inlets and outlets A, B, C and D respectively.

Figure (**5**) shows the effect of the total flow rate on the transfer of sodium fluorescein from inlet B to outlet D. The agreement between the numerical predictions and the experimental data is excellent and highlights the capability of numerical simulation. Figure (**6**) illustrates how the flow rate at outlet C can be optimised to ensure all sodium fluorescein leaves through outlet C. For a total flow rate of 10.2 ml/min (i.e. Q_A = 8.5 ml/min and Q_B = 1.7 ml/min), the numerical results show that Q_C needs to be greater than 3.4 ml/min; this has been confirmed by experiment [60]. Computational Fluid Dynamics (CFD) can therefore significantly reduce experimental effort by avoiding unnecessary trial and error in optimising flow rates.

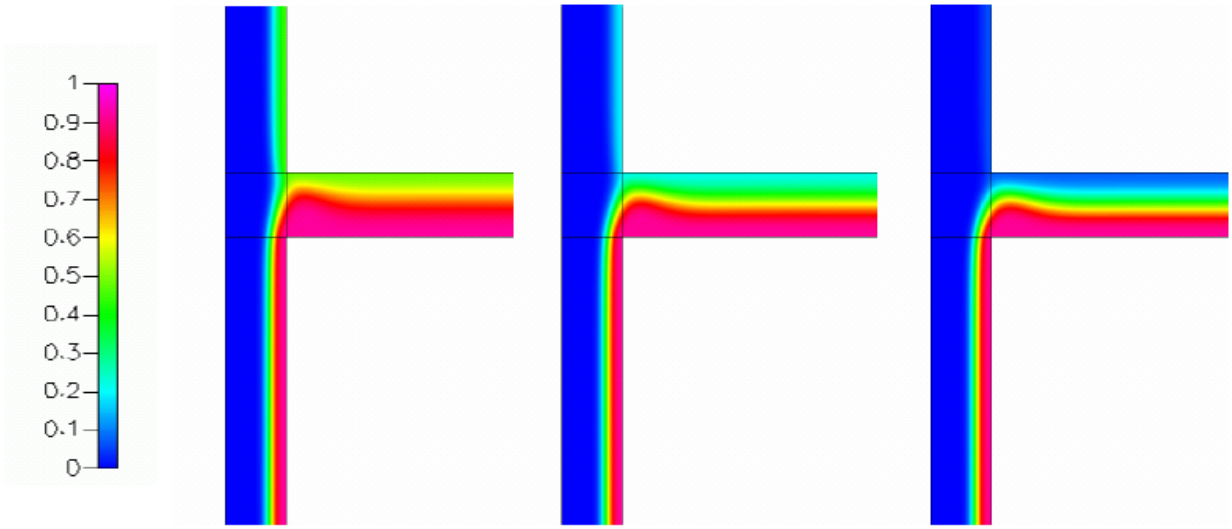

Fig. (**6**). The effect of varying flow rate through outlet C, Q_C, on the transfer of sodium fluorescein: no sound. Simulations carried out using CFD-ACE+ for constant inlet flow rates: Q_A = 8.5 ml/min, Q_B = 1.7 ml/min.

4.2 QUADRUPOLE MAGNETIC FLOW SORTER

Recently, a quadrupole magnetic flow sorter (QMS) has been developed to separate magnetic-bead-tagged cells [61, 62]. As shown in Fig. (**7**), the sample enters the annular separation channel through inlet *a* and the separated particles are collected at outlet *b*. The QMS used by Hoyos et al. [44] has the following geometry: outer radius of separation channel, r_o = 4.53 mm; inner radius of separation channel, r_i = 2.38 mm; inlet splitter radius, r_{sin} = 3.124 mm; and outlet splitter radius, r_{sout} = 3.543 mm. The length of the separation channel between the splitters, L, is 95 mm. The magnet has bore radium of 4.82 mm and a length, L_m, of 76.2 mm. The magnetic flux density at the outer wall r_o is 1.334 T.

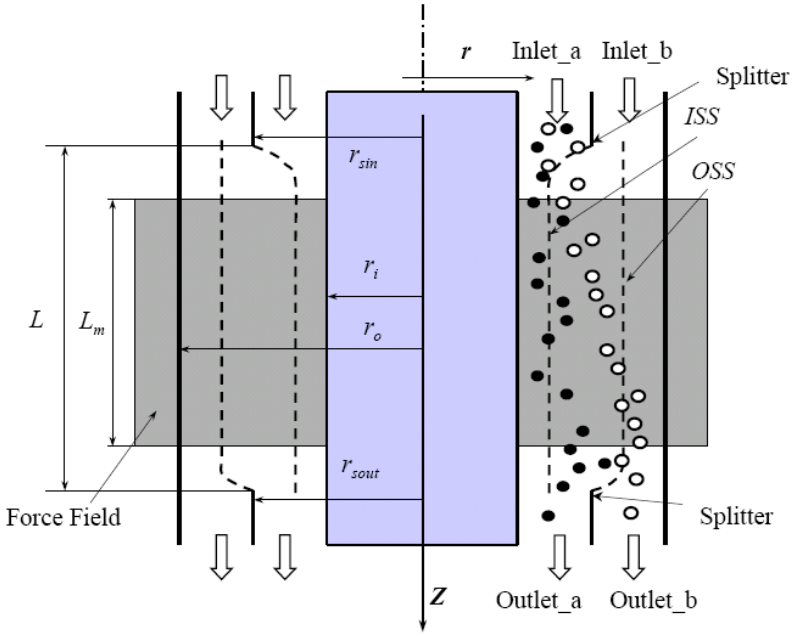

Fig. (**7**). Schematic diagram of an annular quadrupole magnetic flow sorter.

To separate particles with magnetophoretic mobilities of m_{m1} and m_{m2}, the operating flow rates have to be chosen to ensure that all cells with the lower magnetophoretic mobility m_{m1} are collected at outlet *a* while all cells with the higher mobility m_{m2} leave through outlet *b* without sticking to the wall. Therefore, we need to obtain three critical magnetophoretic mobilities: m_0, for a particle trajectory that initially starts at the tip of the splitter at inlet *a* and ends at the splitter at outlet *b* (all particles with mobility smaller than m_0 will leave through outlet *a*); m_1, for a particle trajectory starting at the wall of inlet *a* and ending at the outlet splitter (all particles with mobility greater than m_1 will move across to outlet *b*); and m_2, for a particle trajectory starting from the inlet splitter and just reaching the outlet wall under this critical mobility (all particles with smaller mobility emerging from inlet *a* will not touch the outlet wall. This is important for the separation of fragile cells and to reduce the number of particles sticking to the outer wall thereby increasing the particle retrieval rate). These three critical mobilities are essential for optimising the operating flow rates. The separation of particles with mobilities, m_{m1} and m_{m2}, requires operating flow rates that satisfy the following criteria: $m_{m1} < m_0$ and $m_1 < m_{m2} < m_2$.

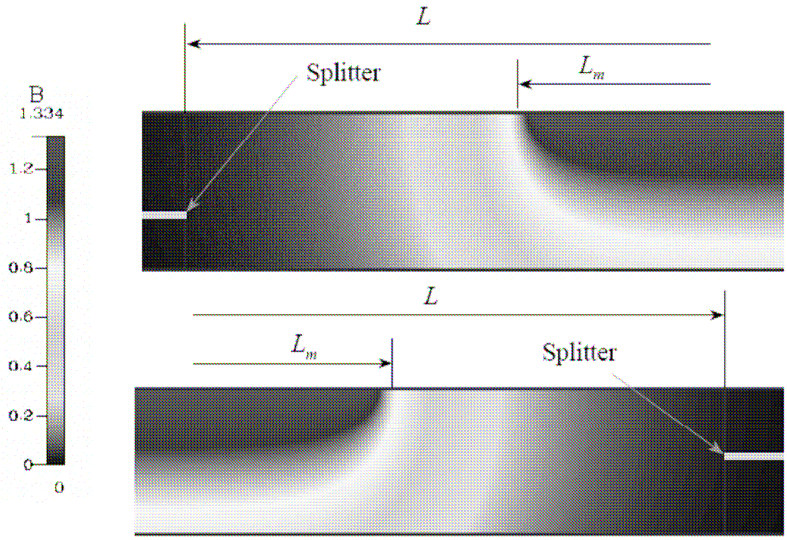

Fig. (**8**). The fringing field of the magnitude of B at the separation channel inlet and outlet, B_0 = 1.334 T. Here, the variation of the fringing field around the circumference of the annular channel is ignored. (Reprinted from ref [53] with permission from Elsevier. Simulations carried out using CFD-ACE+).

In calculating these critical magnetopheretic mobilities, we have to consider other factors such as the effect of the fringing magnetic field in the vicinity of the splitters. The contours of the magnitude of B at the separation channel inlet and outlet are shown in Fig. (**8**). It is clear that the fringing magnetic field causes a gradient in the axial direction i.e. $\partial B / \partial z \neq 0$. Consequently, the applied field will not only have a radial component but also an axial component and therefore it may not always be appropriate to ignore the fringing effect, as detailed in recent work [53].

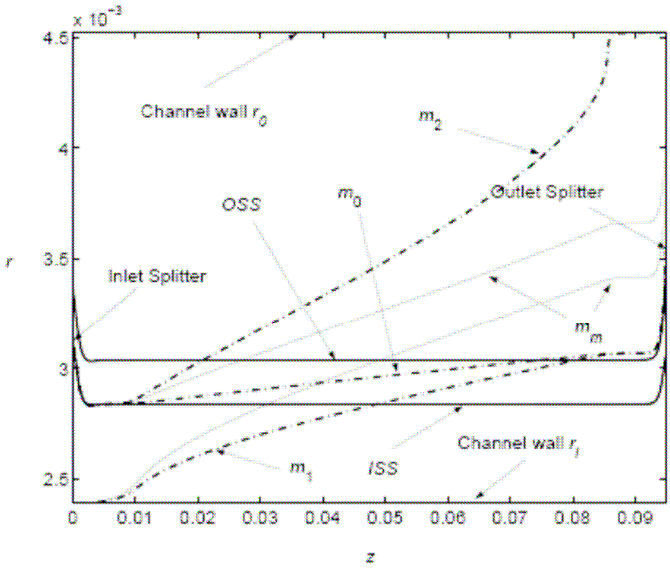

Fig. (**9**). Particle trajectories and inlet splitting streamline (*ISS*) and outlet splitting streamline (*OSS*) in the separation channel. Total flow rate Q = 60 ml/min; magnetic flux density B_0 = 1.334 *T*.
The magnetophoretic mobilities are: $m_0 = 3.98\times10^{-4}$, $m_1 = 8.09\times10^{-4}$, $m_2 = 21.38\times10^{-4}$, and $m_m = 12.0\times10^{-4}$ mm^3/TAs respectively.
(Reprinted from ref [53] with permission from Elsevier.)

Figure (**9**) shows the inlet splitting streamline (*ISS*) and outlet splitting streamline (*OSS*) and the particle trajectories for a total flow rate Q = 60 ml/min and fractional flow rate ratios of $Q_a^{out}/Q = 0.2$ and $Q_a^{in}/Q = 0.1$. Under these operating conditions, the critical mobilities m_0, m_1 and m_2 have been obtained numerically as 3.98×10^{-4}, 8.09×10^{-4} and 21.38×10^{-4} mm^3/TAs, respectively. The corresponding trajectories are shown by the dash-dot lines. If particles with mobility $m_m = 12.0\times10^{-4}$ mm^3/TAs ($m_1 < m_m < m_2$) enter the separation channel through inlet *a*, they will be collected at outlet *b* without sticking to the wall regardless of their initial entry position. The possible trajectories of these particles will lie between the two solid lines marked by m_m. Therefore, the flow rates given above can achieve complete separation of all particles with mobility less than 3.98×10^{-4} mm^3/TAs and greater than 8.09×10^{-4} mm^3/TAs. Ideally, the mobility of the second group of particles should be less than 21.38×10^{-4} mm^3/TAs to avoid problems with the particles sticking to the outer wall of the separation channel.

5. CONCLUSIONS

Microfluidic devices are increasingly being used to separate particles in a wide range of biological and clinical analyses. This review paper focuses on field-flow fractionation (FFF) and split-flow-thin fractionation (SPLITT) and shows how these techniques can be applied to integrated microfluidic systems. The paper provides an overview of the SPLITT fractionation technique and describes the underlying physics which governs the migration of particles under the action of externally applied fields. The paper then illustrates how numerical simulations can be used to provide an increased understanding of the fluid-particle motion along the separation channel. Two recent examples are given that demonstrate the practical potential of numerical simulation; the first considers an ultrasonic cell washing system that can be used to transfer cells or particles from one liquid medium to another (washing), whilst the second example considers the separation of particles of differing magnetophoretic mobilities using a quadrupole magnetic flow sorter. Both examples serve to illustrate how numerical simulations can be used to improve the operating conditions within the device. The use of numerical modelling eliminates the need to perform extensive "trial and error" experiments. For example, numerical modelling can readily investigate a wide range of design parameters including flow rates, channel dimensions, geometries and fluid properties, and can identify key design and operational issues prior to fabrication, considerably reducing the overall development costs. However, it should be emphasized that experimental work is still crucially important for validating the numerical results.

ACKNOWLEDGEMENTS

The authors are grateful to EPSRC (grant reference GR/S82978/01) for supporting this research. In addition, the authors appreciate the useful discussions with Dr. Jeremy Hawkes at the University of Manchester whose suggestions have helped improve this paper.

REFERENCES

[1] Masuda, S.; Washizu, M. and Nanba, T. Proc. Electrostatics, April, 1987, Oxford, p69.

[2] Manz, A.; Graber, N.; Widmer, H.M. Sensor. Actuat. B-Chem., 1990, 1: 244.

[3] Beebe, D. J.; Mensing, G. A.; Walker, G. M. Annu. Rev. Biomed Eng., 2002, 4, 261.

[4] van den Berg, A.; Lammerink, T. Top. Curr. Chem., 1998, 194, 21.

[5] Reyes, D.R.; Iossifidis, D.; Auroux, P.; Manz, A. Anal. Chem., 2002, 74, 2623.

[6] Auroux, P.; Iossifidis, D.; Reyes, D. R.; Manz, A. Anal. Chem., 2002, 74, 2637.

[7] Verpoorte, E. Electrophoresis, 2002, 23, 677.

[8] Vilkner, T.; Janasek, D.; Manz, A. Anal. Chem., 2004, 76, 3373.

[9] Erickson, D.; Li, D. Anal. Chimica Acta, 2004, 507, 11.

[10] Brody, J. P.; Yager, P. Sensors and Actuators A: Physical, 1997, 58, 13.

[11] Yager, P. Transverse diffusion in microfluidic systems, in *Lab-on-a-chip: Chemistry in Miniaturized Synthesis and Analysis Systems*, ed. Oosterbroek, R.E., and van den Berg, A., Elsevier Science: New York, 2003.

[12] Pohl, H.; Kaler, K. Cell Biophys. 1979, 1, 15.

[13] Giddings, J.C. Science, 1993, 260,1456.

[14] Giddings, J.C. Sep. Sci. Tech., 1985, 20, 749.

[15] Springston, S.R.; Myers, M.N.; Giddings, J.C. Anal. Chem., 1987, 59, 344.

[16] Levin S.; Giddings, J.C. J. Chem. Tech. Biotech., 1991, 50, 43.

[17] Fuh, C.B.; Chen, S.Y. J. Chromatogr. A, 1999, 857 (1-2), 193.

[18] Contado, C.; Reschiglian, P.; Faccini, S.; Zattoni, A.; Dondi, F. J. Chromatogr. A 2000, 871, 449.

[19] Cardot, P.; Battu, S.; Simon, A.; Delage, C. J. Chromatogr. B. 2002, 768, 285.

[20] Fuh C.B.; Myers M.N.; Giddings J.C. Anal Chem., 1992, 64 (24), 3125.

[21] Contado, C.; Dondi, F.; Beckett, R.; Giddings, J.C. Anal. Chimica Acta, 1997, 345 (1-3), 99.

[22] Moon, M.H.; Kim, H.J.; Kwon, S.Y.; Lee, S.J.; Chang, Y.S.; Lim, H. Anal. Chem., 2004, 76 (11), 3236.

[23] Williams, P.S.; Levin, S.; Lenczycki, T.; Giddings, J.C. Ind. & Eng. Chem. Res., 1992, 31 (9), 2172.

[24] Fuh, C.B.; Giddings, J.C. J. Microcolumn. Sep., 1997, 9 (3), 205.

[25] Zhang, J.; Williams, P.S.; Myers, M. N.; Giddings, J.C. Sep. Sci. Technol. 1994, 29, 2493.

[26] Fuh, C.B.; Giddings, J.C. Sep. Sci. Tech., 1997, 32 (18), 2945.

[27] Myers, M.N. J. Microcolumn Sep., 1997, 9, 151.

[28] Melville, D.; Paul, F.; Roath, S. IEEE Trans. Magn. Mag., 1975,11, 1701.

[29] Safarik, I.; Safarikova, M. J. Chromatogr. B, 1999, 722, 33.

[30] Corona-Barrera, E.; Smith, D.G.E.; La, T.; Hampson, D.J.; Thomson, J.R. J. Med. Microbiology, 2004, 53 (4), 301.

[31] Zhao, X.Y.; Shippy, S.A. Anal. Chem., 2004, 76 (7), 1871.

[32] Gijs, M. A. M. Microfluid. Nanofluid., 2004, 1, 22.

[33] Moore, L.R.; Zborowski, M.; Sun, L.P.; Chalmers, J.J.. J. Biochem. Bioph. Meth., 1998, 37 (1-2), 11.

[34] Zborowski, M.; Williams, P.S.; Sun, L.; Moore, L.R.; Chalmers, J.J. J. Liq. Chromatogr. R. T., 1997, 20 (16-17), 2887.

[35] Chalmers, J.J.; Zborowski, M.; Sun, L.P.; Moore, L. Biotechnol. Progr., 1998, 14 (1): 141.

[36] Sun, L.P.; Zborowski, M.; Moore, L.R.; Chalmers, J.J. Cytometry, 1998, 33 (4), 469.

[37] Fuh, C.B.; Chen, S.Y. J. Chromatogr. A, 1998, 813 (2), 313.

[38] Fuh. C.B.; Tsai, H.Y.; Lai, J.Z. Anal. Chim. Acta, 2003, 497 (1-2), 115.

[39] Zborowski, M.; Sun, L.P.; Moore, L.R.; Williams, P.S.; Chalmers, J.J. J. Magn. Magn. Mater., 1999, 194 (1-3), 224.

[40] Nakamura, M.; Decker, K.; Chosy, J.; Comella, K.; Melnik, K.; Moore, L.; Lasky, L.C.; Zborowski, M. Biotechnol. Progr., 2001, 17 (6), 1145.

[41] Wingo, R.M.; Prenger, F.C.; Johnson, M.D.; Waynert, J.A.; Worl, L.A.; Ying, T.Y., Sep. Sci. Tech., 2004, 39, 2769.

[42] Fuh, C.B.; Lai, J.Z.; Chang, C.M. J. Chromatogr. A, 2001, 923 (1-2), 263.

[43] Fuh, C.B.; Su, Y.S.; Tsai, H.Y. J. Chromatogr. A, 2004, 1027 (1-2), 289.

[44] Zborowski, M.; Ostera, G.R.; Moore, L.R.; Milliron, S.; Chalmers, J.J.; Schechter, A.N. Biophys. J., 2003, 84 (4), 2638.

[45] Hoyos, M.; Moore, L.R.; McCloskey, K.E.; Margel, S.; Zuberi, M.; Chalmers, J.J. J. Chromatogr. A, 2000, 903 (1-2), 99.

[46] Williams, P.S.; Zborowski, M.; Chalmers, J.J. Anal. Chem., 1999, 71 (17), 3799.

[47] Watarai, H; Namba, M.J. Chromatogr. A, 2002, 961 (1), 3.

[48] Moore, L.R.; Milliron, S.; Williams, P.S.; Chalmers, J.J.; Margel, S.; Zborowski, M. Anal. Chem., 2004, 76 (14), 3899.

[49] Williams, P.S.; Moore, L.R.; Chalmers, J.J.; Zborowski, M. Anal. Chem., 2003, 75 (6), 1365.

[50] Williams. P.S.; Decker, K.; Nakamura, M.; Chalmers, J.J.; Moore, L.R.; Zborowski, M. Anal. Chem., 2003, 75 (23), 6687.

[51] Williams, P.S. Sep. Sci. Tech., 1994, 29, 11.

[52] Zhang, Y.H.; Emerson, D.R.; Reese, J.M. J. Chromatogr. A, 2003, 1010, 87.

[53] Zhang, Y.H.; Emerson, D.R. J. Chromatogr. A, 2004, 1042, 137-145.

[54] Hunter R.J. Foundations of Colloid Science, Oxford University Press: Oxford, 2001.

[55] Saffman, P.G. J. Fluid Mech. 1968, 31, 624.

[56] Fan, L.S.; Zhu, C. Principles of Gas-Solid flows, Cambridge University Press, Cambridge, 1998.

[57] Knoepfel, H.E. Magnetic fields: a comprehensive theoretical treatise for practical use, John Willey & Sons, New York, 1999.

[58] Elghogashi, S.E. Appl. Sci. Res., 1994, 52, 309.

[59] CFD Research Corporation, Cummings Research Park, 215 Wynn Drive, Huntsville, AL 35805, USA, User Manual: Version 6.4, 2000.

[60] Hawkes, J.J.; Barber, R.W.; Emerson, D.R.; Coakley, W.T. Lab. Chip, 2004, 4, 446.

[61] Moore, L.R.; Rodriguez, A.R.; Williams, P.S.; McCloskey, K.; Bolwell, B.J.; Nakamura, M.; Chalmers, J.J.; Zborowski, M. J Magn. Magn. Mater., 2001, 225 (1-2): 277.

[62] Hoyos, M.; McCloskey, K.E.; Moore, L.R.; Nakamura, M.; Bolwell, B.J.; Chalmers, J.J. Sep. Sci. Tech., 2002, 37 (4), 745.